Journal of Power Sources 199 (2012) 386–394

Contents lists available at SciVerse ScienceDirect

Journal of Power Sources

journal homepage: www.elsevier.com/locate/jpowsour

Electrostatic self-assembly of hierarchical porous carbon microparticles

Juan Balach[a], Mariano M. Bruno[b], N. Gustavo Cotella[a], Diego F. Acevedo[a], César A. Barbero[a,*]

[a] Programa de Materiales Avanzados, Universidad Nacional de Río Cuarto, Agencia Postal No. 3, 5800 Río Cuarto, Argentina
[b] Departamento de Física de la Materia Condensada, Centro Atómico Constituyentes, Comisión Nacional de Energía Atómica (CNEA), General Paz 1499, 1650 San Martín, Buenos Aires, Argentina

ARTICLE INFO

Article history:
Received 7 October 2011
Accepted 9 October 2011
Available online 14 October 2011

Keywords:
Hierarchical
Porous carbon
Mesoporous
Self-assembly
Supercapacitor
Pseudocapacitance

ABSTRACT

Hierarchical porous carbon microparticles (HPCMs) are produced by milling and sieving porous monolithic carbon, which was obtained by carbonization of a resorcinol-formaldehyde gel in the presence of surfactant as a pore stabilizer. The obtained HPCMs has a surface area of 536 $m^2 g^{-1}$ and maximum specific capacitance and areal capacitance, measured at slow scan rates, of 194 $F g^{-1}$ and 152 $mF cm^{-2}$ respectively. Moreover, the carbon surface remains accessible at 100 $mV s^{-1}$ with large values of specific capacitance (154 $F g^{-1}$) and areal capacitance (121 $mF cm^{-2}$), making the material suitable for fast supercapacitors. The HPCMs are then built into electrostatic self-assembled (ESA) adsorbed layers by sequential immersion of a planar electrode in HPCMs dispersions and a cationic polyelectrolyte. Using soluble redox molecules, it is possible to detect the finite (inside the pores) and semi-infinite (outer surface) diffusion of redox species. The specific capacitance of the HPCMs could be increased up to 5 times (to ca. 900 $F g^{-1}$ in acid media) by adsorption of naphthoquinone molecules on the carbon surface. Using the ESA process, it is possible to build a layer with three different quinones in a single electrode. The specific capacitance of those layers is more than 4 times higher and maintained nearly constant in a wide range of potential.

1. Introduction

Porous carbon could be used as electrode materials of electrochemical supercapacitors due to its intrinsic electric conductivity, good chemical stability and large surface area [1,2]. Different procedures have been devised to produce carbon with large surface area, including activation of compact porous materials [3], fabrication of aerogels [4], or creation of porous carbon by use of hard [5], or soft templates [6]. The process of charging and discharging of the supercapacitor requires the transport of ions inside the pores. To achieve large surface areas (>500 $m^2 g^{-1}$) the diameter of the pores should be small (<50 nm). If the pores depth is large (>100 μm) the mass transport will make the capacitor response slow. To overcome such constraint, the length of the pores should be decreased. This can be done by fabrication of thin films supported on conducting fibers [7] or by building the electrode using small microparticles. A simple procedure to assemble materials onto solid surfaces was introduced first by Iler [8] and rediscovered by Decher et al. [9,10]. The Decher's method involves the immersion of the surface, which bears a permanent surface charge due to chemical groups present at the surface, in solution of polyelectrolytes. By alternate immersion in solutions of polylelectrolyte, with an intermediate washing step to remove non adsorbed material, multilayers of polymers can be built. While the electrostatic charge compensation plays a role on the adsorption, other factors are involved such as removal of mobile counterions [11] and attraction by dispersion forces [12]. The methods have been used to assemble nanoparticles [13], including carbon nanotubes [14]. In this case, the main attraction force that maintains the multilayer together involves dispersion forces between particles because the surface charge density is much smaller in nanoparticles than in macromolecules. In that way, the contribution of electrostatic attraction or counterion removal to the thermodynamic spontaneity of the process becomes smaller. Moreover, any stable colloidal dispersion could be used as source of material for the assembly. Serizawa et al. [15], adsorb monolayers of relatively large (548 nm) polystyrene nanoparticles onto a charged multilayer showing that stable adsorption can be achieved. Lyon et al. [16] adsorb charged hydrogel nanoparticles by Decher's method but found that bidimensional coverage is obtained instead of multilayers. In the present work, Decher's method is used to self-assemble porous carbon microparticles onto conductive surfaces. Each microparticle has large specific capacitance due to the large surface area of the porous structure. At the same time, using small microparticles it is possible to maintain the maximum length of the pores small to allow fast response. The electrolyte access the external surface of the microparticles trough the interstitial space between particles. The procedure could be used to build small supercapacitors and to study the amount of charge that could be stored in each microparticle. Since we observe that we do not

* Corresponding author. Tel.: +54 358 4676233; fax: +54 358 4676233.
E-mail addresses: jbalach@gmail.com (J. Balach), cbarbero@exa.unrc.edu.ar (C.A. Barbero).

0378-7753/$ – see front matter © 2011 Elsevier B.V. All rights reserved.
doi:10.1016/j.jpowsour.2011.10.029

build multilayers but increase the coverage of the surface in each adsorption step, we call the procedure step-by-step.

2. Materials and methods

2.1. Synthesis of porous carbon microparticles

Precursor porous gel was prepared by sol–gel polycondensation of resorcinol (R) with formaldehyde (F) in the presence of surfactant as a pore stabilizer [17]. In this study, sodium carbonate (C) and cationic surfactant, cetyltrimethylammonium bromide (CTAB), were used as a basic catalyst and a pore former, respectively. The molar ratio of resorcinol, formaldehyde (37 wt%, in an aqueous solution stabilized by 10% methanol) and CTAB was 1:2:0.06. The molar ratio of sodium carbonate to resorcinol was 600:1 and the ratio of resorcinol to water was 1:2 g ml^{-1}. The mixtures were stirred and heated over at 303 K to promote the surfactant micellization. Then the sample was placed in Petri dish closed inside a closed glass receptacle with water saturated atmosphere and formaldehyde at temperature of 343 K for 24 h to obtain monolithic organic gel. The organic polymeric gel was dried at ambient pressure and room temperature for several days. The dry monolithic gel was converted into monolithic carbon by carbonization at 1073 K for 1 h under an argon atmosphere with a heating rate of 313 K h^{-1}. Finally, hierarchical porous carbon microparticles (HPCMs) down to 25 μm size were obtained by milling and sieving the monolithic carbon.

2.2. Preparation of electrodes

The working electrodes were prepared by coating Nafion-carbon ink onto a vitreous glassy carbon electrode in order to obtain a film-coated electrode. Three different of carbon inks for the electrochemical capacitance studies were prepared as follows: (ink-1) 20 mg of HPCMs as active material was mixed with 0.5 ml of deionized water, 0.5 ml ethanol and 0.3 ml of Nafion solution (5 wt%, DuPont), (ink-2) 20 mg of commercial graphite as conducting agent was added to ink-1, and (ink-3) for a comparison, commercial graphite was also used as active material to prepare film-coated electrode under the same condition of ink-1. These mixtures were ultrasonicated for 60 min to form a homogenous ink. Finally, 12.5 μl of the resulting ink was then deposited by drop-coating on a glassy carbon electrode (1.5 cm^2) and dried at 323 K for 10 min. The average area of the active film-coated electrode was 0.288 ± 0.028 cm^2.

ITO glasses were used as electrodes for alternate electrostatic self-assembly (ESA) adsorption. ITO electrodes were cleaned with ethanol, then with deionized water and finally heated for 1 h in the furnace at 723 K in air.

2.3. Physical characterization and electrochemical tests

The nitrogen sorption isotherm curve was measured using an ASAP 2020 (Micrometrics) system. Porosity analysis was carried out at liquid nitrogen temperature, 77 K. BET surface area (S_{BET}) was calculated using the Brunauer–Emmett–Teller (BET) theory [18]. Mesopore size distribution (d_{meso}) was determined by Barrett–Joyner–Halenda (BJH) method [19]. Micropore size distribution (d_{mic}) was calculated using nonlinear density functional theory (NLDFT) method [20], assuming slit pore shape. Carbon morphology was observed using a scanning electron microscope (FEI Helios Nanolab 600).

The cyclic voltammetry (CV) tests for capacitance studies were carried out at different scan rates in 1 M H_2SO_4 in an aqueous media using a conventional three-electrode cell. A monolithic mesoporous carbon (geometrical area 10 times larger than the working electrode and a rugosity >50.000) was used as a counter electrode. A silver/silver chloride electrode (saturated KCl) was used as a reference electrode. CV was performed using a PC4 Potentiostat–Galvanostat–ZRA (Gamry Instruments, Inc.). In the resulting cyclic voltammograms the current was divided by the scan rate and the electrode mass to obtain specific capacitance versus voltage profiles. Electrochemical impedance spectroscopy (EIS) of the samples was measured in 1 M H_2SO_4 solution over the frequency range from 1×10^4 Hz to 2.8×10^{-3} Hz at 0.35 V, with sinusoidal perturbation of 1 mV of amplitude and 4 points per decade change in frequency. A resting time of 15 min (at 0.35 V) was used before each measure. The specific capacitance obtained by CV tests was calculated by $C_{CV} = i/\nu m$, where i is the current, ν is the scan rate and m is the mass of HPCMs deposited on the glassy carbon electrode. The specific capacitance obtained by EIS from the data at the lowest frequency was evaluated by $C_{EIS} = -1/2\pi f Z'' m$, where Z'' is the value of the imaginary part obtained from the frequency f of disturbance. Specific capacitances of carbon samples were converted to areal capacitance (capacitance per geometrical area) considering the area of film-coated electrode.

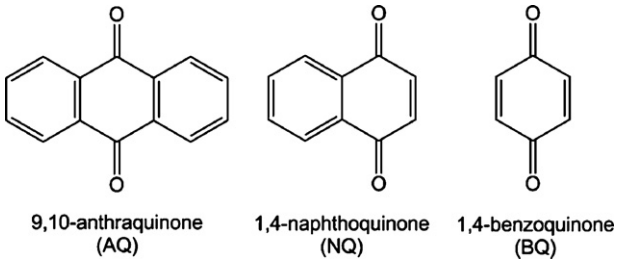

Fig. 1. Chemical structures of 9,10-anthraquinone, 1,4-naphthoquinone and 1,4-benzoquinone.

2.4. ESA procedure

The ITO electrodes were immersed (10 min each) successively in solutions of the polydialyldimethylammonium chloride (PDADMAC) (2% (w/v) in deionized water) and HPCMs (0.5% (w/v) in phosphate buffer 0.1 M, pH 7). Between immersions, the electrodes were washed by immersing for 5 min in deionized water, without stirring. This cycle process was repeated until reach the desired numbers of adsorptions. It is know that it is possible adsorb spontaneously PDADMAC on the substrate surface to produce a first charged layer on ITO [14]. Therefore, no covalent modification of the electrode surface was necessary. PDADMAC and HPCMs were used as polycation and negative charged particles, respectively. Adsorption of different quinones on a modified electrode with PDADMAC and HPCMs was also performed. The quinones chosen were 1,4-naphthoquinone (NQ), 9,10-anthraquinone (AQ) and 1,4-benzoquinone (BQ). The chemical structures of used quinones are shown in Fig. 1. After obtaining 2, 4 and 6 adsorption cycles of PDADMAC and HPCMs, the electrode was immersed for 30 min in a quinone solution. Then the electrode doped with quinones was immersed in a 1 M $HClO_4$ aqueous solution for 80 min, in order to remove the quinones not adsorbed into the pore. CV measurements were performed in 1 M $HClO_4$ solution. Redox molecules as $K_4Fe(CN)_6$ was also used as probe molecules.

2.5. Optical microscopy

Optical micrographs of the self-assembled surfaces were obtained by an optical microscope (Arcano XZF145), with a Motic 2000 digital camera. The images were analyzed by the Motic Image Plus 2.0 ML software. All operations were performed at room temperature.

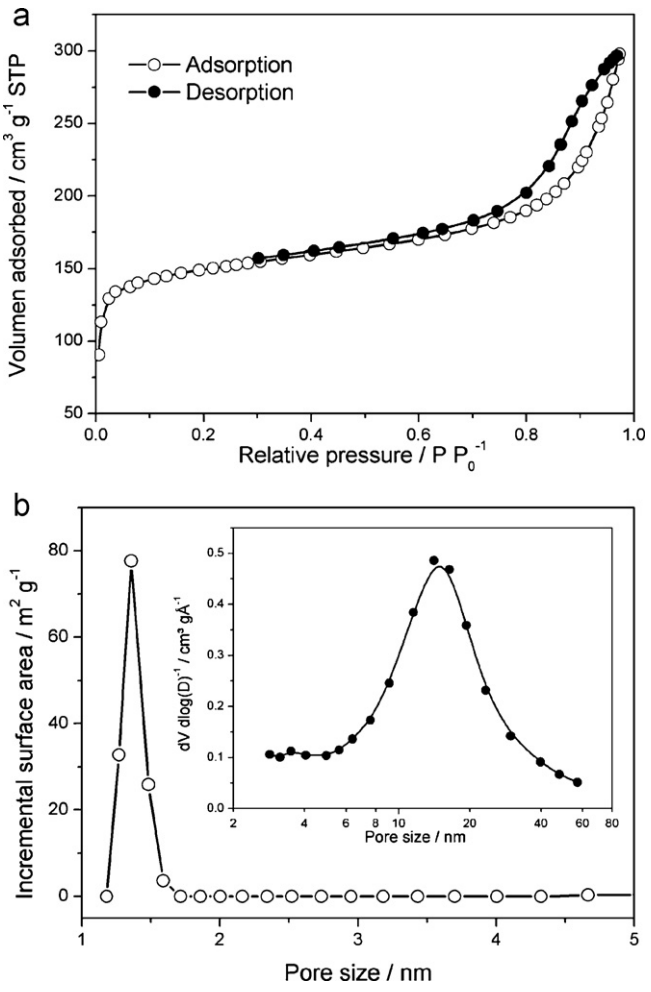

Fig. 2. (a) Nitrogen adsorption–desorption isotherm of carbon microparticles sample. (b) NLDFT and BJH (inset) pore size distribution curves obtained from (a).

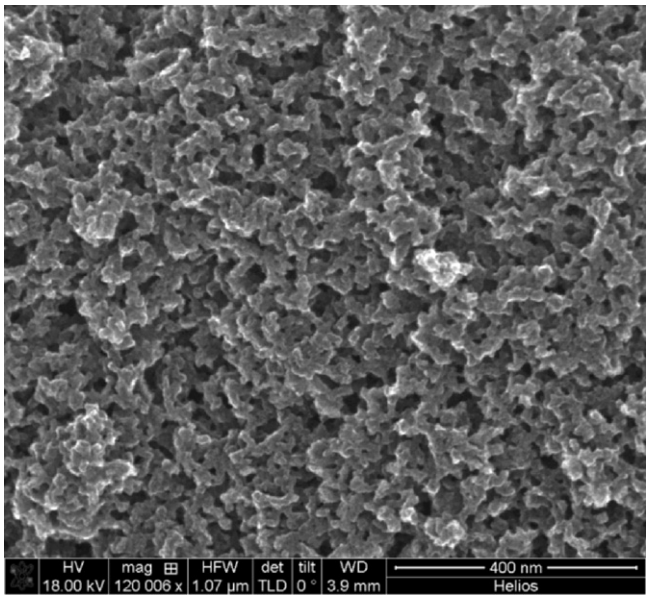

Fig. 3. SEM micrograph of the surface of HPCM sample.

3. Results and discussion

3.1. Textural properties and surface morphology

Fig. 2 presents the nitrogen adsorption–desorption isotherm of HPCMs and pore size distribution derived from the desorption branch of the isotherm. The parameters of surface area and porosity are summarized in Table 1. The adsorption belongs to a type-IV isotherm, indicating the presence of mesoporous in the carbon material. The measured BET surface area is 536 $m^2\,g^{-1}$. The NLDFT pore size distribution plots (Fig. 2b) presents a d_{mic} of 1.35 nm of diameter, whereas the BJH d_{meso} distribution plots (inset in Fig. 2b) determined from desorption branch of the isotherm presents a maximum at 15 nm of diameter. Both pores size are a decisive factor influencing the capacitance [21] and rapid access of electrolyte to the electrode material, that is, HPCMs.

Surface morphology of HPCMs was examined by SEM. Fig. 3 shows the SEM images on the external surface of the HPCMs obtained using CTAB as a pore stabilizer. The SEM image (Fig. 3) shows a porous structure with pores uniformly distributed. Also it is possible to observe that the size of external pores is larger than mesopore size distribution obtained by BJH method (inset in Fig. 2b). This means that HPCMs has three different classes of pores (micro- meso- and macroporous) [22] making it this kind of carbon material, a hierarchical porous carbon.

In order to obtain the percentage of micro- meso- and macopores of carbon sample, we first calculated the total pore volume of HPCM (V_{tot}) by [23]:

$$V_{tot} = \rho_{HPCM}^{-1} - \rho_{compact}^{-1} \quad (1)$$

where $\rho_{compact}$ is the density of non-porous carbon (compact carbon) with a value of 2.2 $g\,cm^{-3}$ [24], and ρ_{HPCM} is the apparent density, measured from the ratio of weight to geometric volume, is $0.89 \pm 0.01\,g\,cm^{-3}$.

From the calculated value of V_{tot}, which is 0.669 $cm^3\,g^{-1}$, and taking a count the V_{meso} and V_{mic} obtained by nitrogen sorption isotherm measurement (see Table 1), is possible to calculate the macropore volume ($=V_{tot} - V_{meso} - V_{mic}$), and to estimate the percentage of micropores, mesopores and macropores that presents the HPCMs, which are 25.3%, 43.6% and 31.1%, respectively. The presence of large pores in HPCMs sample indicates that a pore former effect by the surfactant is operative.

3.2. Capacitance performance of HPCMs

CV and EIS measurements were carried out in order to examine the electrochemical properties of commercial graphite, HPCMs and HPCMs with graphite and shown in Fig. 4. The comparative CV plots of HPCMs and HPCMs with graphite at various scan rates are shown in Fig. 4a. The typical rectangular shape of the cyclic voltammogram curve shows that the carbon sample is capacitive and highly reversible, as expected for an ideal electrochemical double layer capacitor (EDLC). However, the specific capacitance of HPCMs with graphite is higher than that of HPCMs without graphite. Due to that the voltammogram at a scan rate of 100 $mV\,s^{-1}$ reveals a specific capacitance of ca. 8 $F\,g^{-1}$, 100 $F\,g^{-1}$ and 155 $F\,g^{-1}$ at 0.35 V, for graphite, HPCMs and HPCMs with graphite samples, respectively, the extra capacitance of HPCMs with graphite comes from the fact that the graphite connects electrically better the particles of HPCM. These results means that the well-connected network pores of the hierarchical porous carbon plays an important role in promoting fast electrolyte adsorption/desorption from the bulk solution toward the inside of the porous carbon and the addition of carbon graphite could significantly improve the electron transport of film-coated electrode. The fast kinetics of electrolyte adsorption/desorption can be confirmed by the results

Table 1
Surface texture properties of HPCMs.

Sample	S_{BET} ($m^2\ g^{-1}$)	S_{mic} ($m^2\ g^{-1}$)	V_{meso} ($cm^3\ g^{-1}$)	V_{mic} ($cm^3\ g^{-1}$)	d_{mic} (nm)	d_{meso} (nm)
HPCMs	536	473	0.292	0.169	1.35	15

S_{BET}, BET surface area; S_{mic}, micropore surface area; V_{meso}, mesopore volume; V_{mic}, micropore volume, d_{mic}, micropore size distribution; d_{meso}, mesopore size distribution.

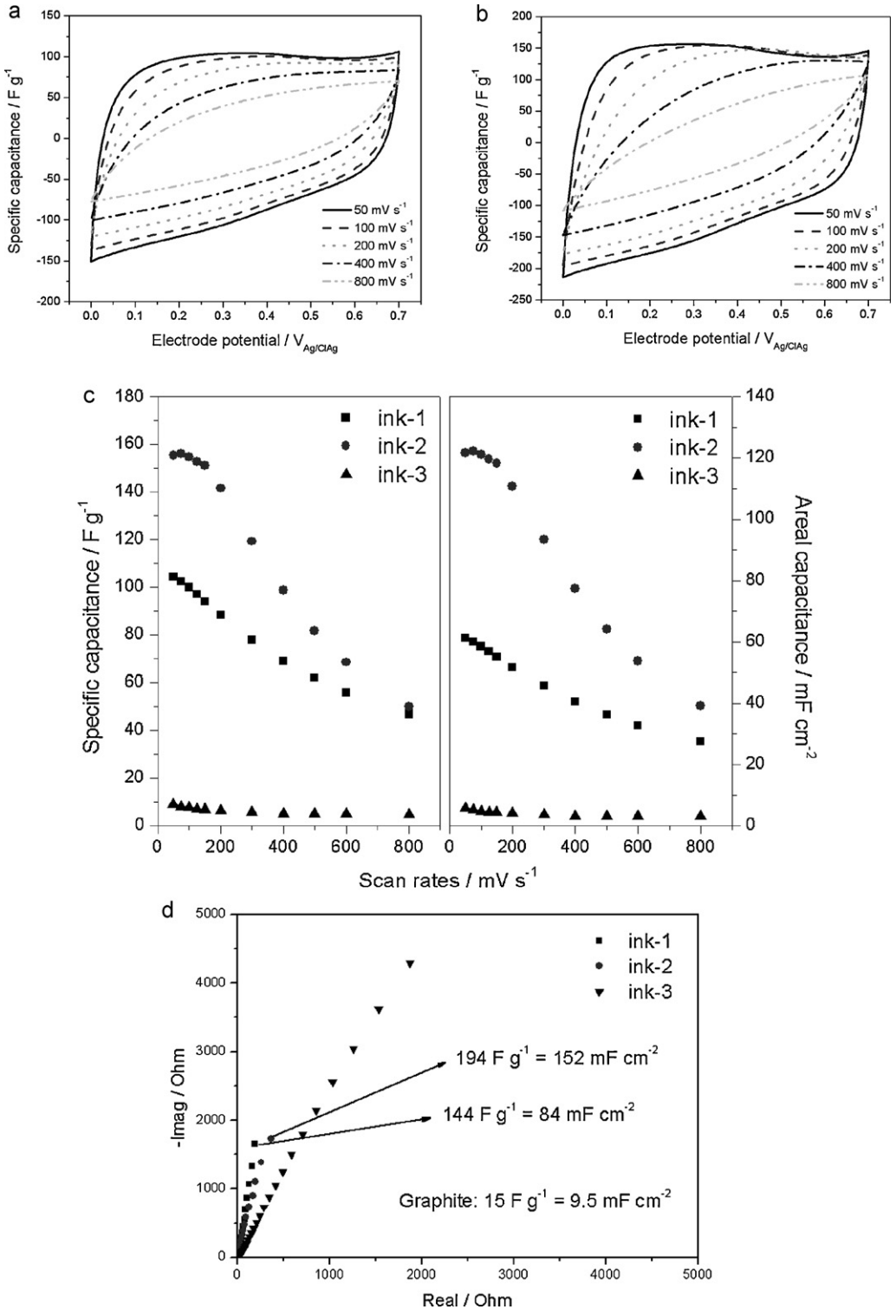

Fig. 4. Electrochemical properties of HPCMs (ink-1), HPCMs with graphite (ink-2) and commercial graphite (ink-3). Cyclic voltammogram at different scan rates of (a) HPCMs, and (b) HPCMs with graphite, (c) specific capacitance and areal capacitance of graphite, HPCMs and HPCMs with graphite at different scan rates and (d) Nyquist plot for graphite, HPCMs and HPCMs with graphite. Frequency range is 10×10^3 to 2.8×10^{-3} Hz.

Table 2
Specific capacitance and areal capacitance of HPCMs, HPCMs with graphite and commercial graphite.

Sample	Specific capacitance ($F g^{-1}$)		Areal capacitance ($mF cm^{-2}$)	
	CV[a]	EIS	CV[a]	EIS
HPCMs	100	144	58	84
HPCMs with graphite	154	194	121	152
Graphite	8	15	5	9.5

[a] Specific capacitance and areal capacitance obtained at 100 mV s^{-1} and at 0.35 V.

obtained from Fig. 4b at a relatively high scan rate of 400 mV s^{-1}, where the sample shown a specific capacitance of ca. 100 F g^{-1} at 0.35 V.

Fig. 4b shows the rate performance of areal capacitance. The specific capacitance and areal capacitance obtained by CV and EIS for all samples is compiled in Table 2 for easy comparison. It can be seen that the HPCMs with graphite have a high areal capacitance of ca. 121 mF cm^{-2} at a relatively high scan rate of 100 mV s^{-1}. The areal capacitance for HPCMs with graphite reaches values of 152 mF cm^{-2} when it is obtained by EIS measurement at low frequencies (Fig. 4d). At higher scan rates, not all the pores area accessible and the value of the specific capacitance decreased.

Some authors report the specific capacitance per BET surface area, but does not include information about density of carbon material, which makes it difficult to estimate the volume occupied by the carbon in an electronic device. We consider that it is more appropriate to report the areal capacitance because the energy stored per area is more relevant than energy per mass for applications such as small scale electronics or stationary energy store devices [25].

3.3. ESA of carbon microparticles

A method that allows adsorb the minimum requisite amount of material onto an electrode is the electrostatic self-assembly procedure, allowing reduce costs in the electrode modification process. Successive cycles of ESA adsorption using PDADMAC and HPCMs on ITO electrode were realized. After each immersion into PDADMAC solution and HPCMs suspension, it is possible to visualize with naked eye that black coloration increases. This indicates that the amount of HPCMs adsorbed on the electrode is increasing (PDADMAC is colorless). This fact is confirmed by CV. The cyclic voltammograms (Fig. 5) shows that the capacitive current increases with each adsorption cycles. It also can be seen that the current increases linearly with the number of steps (inset in Fig. 5). As PDADMAC is not conductive, all capacitive current is obtained from HPCMs. This behavior suggests that carbon microparticles are connected electrically between them and/or with the surface of base electrode.

Stepwise adsorption cycles of HPCMs on ITO glass were followed by optical microscopy. As can be seen in Fig. 6, the carbon particle density increase with each deposited cycle. Fig. 6a, corresponding to third adsorption cycle, shows a sparse distribution of particles due coulombic repulsion between particles. This behavior can be seen in the first and second adsorption cycle (not shown here). After successive adsorption cycles of HPCMs, a moderate improvement in the homogeneity is observed (Fig. 6d). A schematic drawing of the ESA adsorption process is shown in Fig. 7. This result can be explained considering that PDADMAC coat the surface of HPCMs, neutralizing and reversing the charge on the particles, allowing van der Waals interaction between them.

The stepwise adsorption cycles can be characterized by evaluating the normalized surface coverage (C_s) by the analysis of the optical image. In this study, the C_s is defined as the percentage ratio of the occupied area of particles on a unit area per the same unit area. In Fig. 8, current at 0.3 V obtained from Fig. 5 is plotted against C_s for the number of adsorption cycles. The maximum of C_s reaches 56% obtained after 12 adsorption cycles. This result correlate well with the maximum coverage of latex spheres distributed on a surface [15,26].

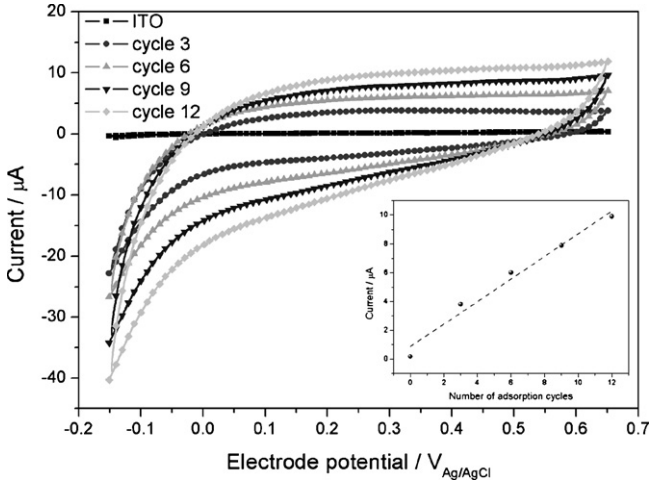

Fig. 5. Cyclic voltammograms of PDADMAC/HPCMs. Electrolyte: 1 M $HClO_4$. Scan rate: 50 mV s^{-1}. The alternated adsorption cycles are deposited on ITO glass as a base electrode. The inset shows the plot of current (at 0.3 V) versus number of adsorption cycles.

3.4. Effect of ESA of carbon microparticles on soluble redox couple electrochemistry

The current due to a redox reaction, such as $[Fe(CN)_6]^{4-}$ oxidation/reduction, could be used to measure the exposed area of the HPCMs deposited during the ESA process. The cyclic voltammograms (Fig. 9) show an increase of the oxidation current at ca. 0.257 V with each adsorption cycle. The voltamogram not only shows the characteristic oxidation-reduction peak of the probe molecule at 0.257 V expected for electrochemical reaction of a redox couple: $[Fe(CN)_6]^{4-}/[Fe(CN)_6]^{3-}$, but also a new peak system at 0.090 (anodic) and 0.080 V (cathodic). The peak system is at a lower potential than the one for the peak of semi-infinite diffusion. This result suggest that the redox probe could be absorbed into the pores of carbon, being able to be oxidized and reduced at the standard potential of the couple, without diffusional overpotential [27]. To check that model, we study the effect of scan rate (from 10 to 150 mV s^{-1}) on the peak currents.

Fig. 9b shows two different dependences of the peak currents with the scan rate. To allow comparison, we plot the logarithm(ip) as a function of log(ν). The plot of the anodic currents measured at 0.257 V show a linear slope of 0.49 ± 0.02 indicating that the peak current for $[Fe(CN)_6]^{4-}$ oxidation is proportional to the square root of the scan rate. Therefore, the redox couple is oxidized under conditions of semi-infinite diffusion [28]. The plot of the peak current measured at 0.090 V show a slope of 1.06 ± 0.04, suggesting that the peak current is linearly dependent on scan rate. Therefore $[Fe(CN)_6]^{4-}$ is oxidized under conditions of finite diffusion [27]. These results suggest that redox probe is both confined within the pore of HPCMs and present in the bulk solution. It has to be bear in mind that the same soluble redox couple probe the two different diffusion condition but no significant adsorption of $[Fe(CN)_6]^{4-}$ on the carbon surface occurs.

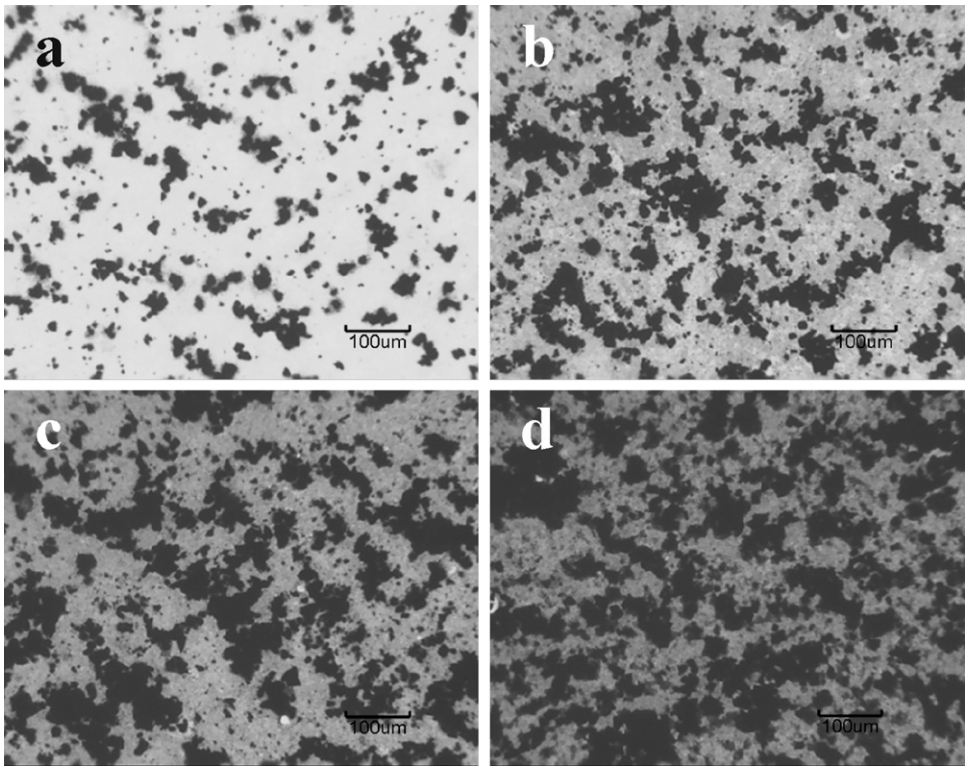

Fig. 6. Micrographs corresponding to (a) third, (b) sixth, (c) ninth and (d) twelfth of successive alternated adsorption cycles of PDADMAC and HPCMs on ITO glass.

3.5. *Effect of ESA of carbon microparticles on adsorbed couple electrochemistry*

The possibility to adsorb different redox couples on the carbon surface was studied using 1,4-naphthoquinone (NQ), 9,10-anthraquinone (AQ) and 1,4-benzoquinone (BQ).

Fig. 10a shows the cyclic voltammograms of PDADMAC/HPCMs measurements in 1 M $HClO_4$ solution. The current at 0.278 V increases ca. 4.7 times compared to the sixth adsorption cycles of PDADMAC/HPCMs, when NQ is adsorbed by immersion of the electrode in a 10 mM NQ acetonitrile solution. To determine if the NQ is adsorbed into the pore of the HPCMs, the effect of scan rate (from 10 to 150 mV s^{-1}) on the response was studied (Fig. 10b).

As can be seen in Fig. 10b, the logarithmic of anodic currents at 0.278 V versus logarithmic of scan rate has a slope of 0.96 ± 0.02, indicating that NQ is oxidized under conditions of finite diffusion [27]. This indicates that NQ is adsorbed on the HPCMs. While it is possible for NQ to be adsorbed only on the outer surface area of the particles, a comparison of the capacitance of the clean electrode (cycle 6), due only to double layer charging with the pseudo-capacitance due to adsorbed NQ, suggest that NQ is adsorbed on the whole surface are of the HPCMs.

Due that is possible to adsorb NQ on the HPCMs, now we used the ESA process to adsorb NQ every three adsorption cycles of PDADMAC/HPCMs. Fig. 11 shows the third, sixth and ninth adsorption cycles of PDADMAC/HPCMs with adsorbed NQ.

As can be seen in Fig. 11, the current at 0.280 V increases with adsorption cycles process. It also can be seen that the current increases linearly with the number of steps (inset in Fig. 11). This means that modified electrode shows the redox response of NQ, which is adsorbed on the HPCMs.

Since it was possible to successfully adsorb NQ on a modified electrode, it is possible to adsorb AQ following the same protocol. In this case, after every three adsorption cycles of PDADMAC/HPCMs, the electrode was immersed for 30 min in a 10 mM AQ alcohol–water solution. Fig. 12 shows the obtained voltammograms of the third, sixth and ninth adsorption cycles of PDADMAC/HPCMs after adsorbing AQ.

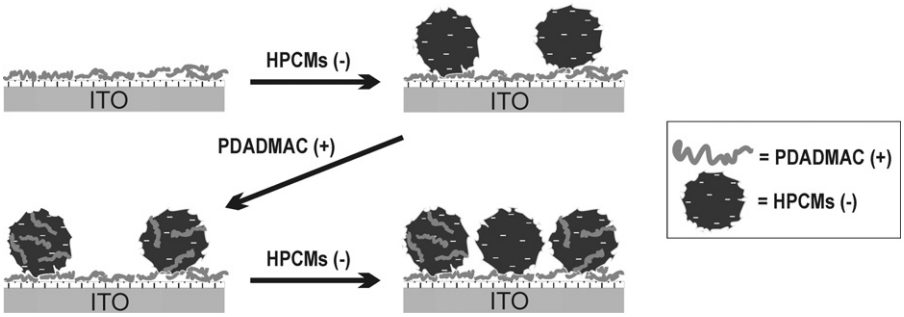

Fig. 7. Schematic drawing of ESA process. The first adsorption of HPCMs showed (previous adsorption of PDADMAC) the particles are located randomly separated from each other. The subsequent adsorption of PDADMAC onto HPCMs leads to a neutralization/inversion of the surface charge of adsorbed particles, allowing the next adsorption of HPCMs are placed between the particles coated with PDADMAC.

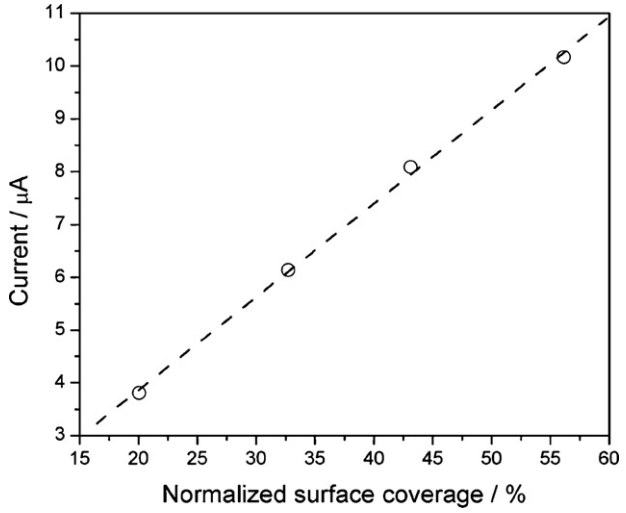

Fig. 8. Plot of current obtained from Fig. 4 versus normalized surface coverage (C_s) of PDADMAC and HPCMs on ITO glass. The experimental points correspond to third, sixth, ninth and twelfth adsorption cycle.

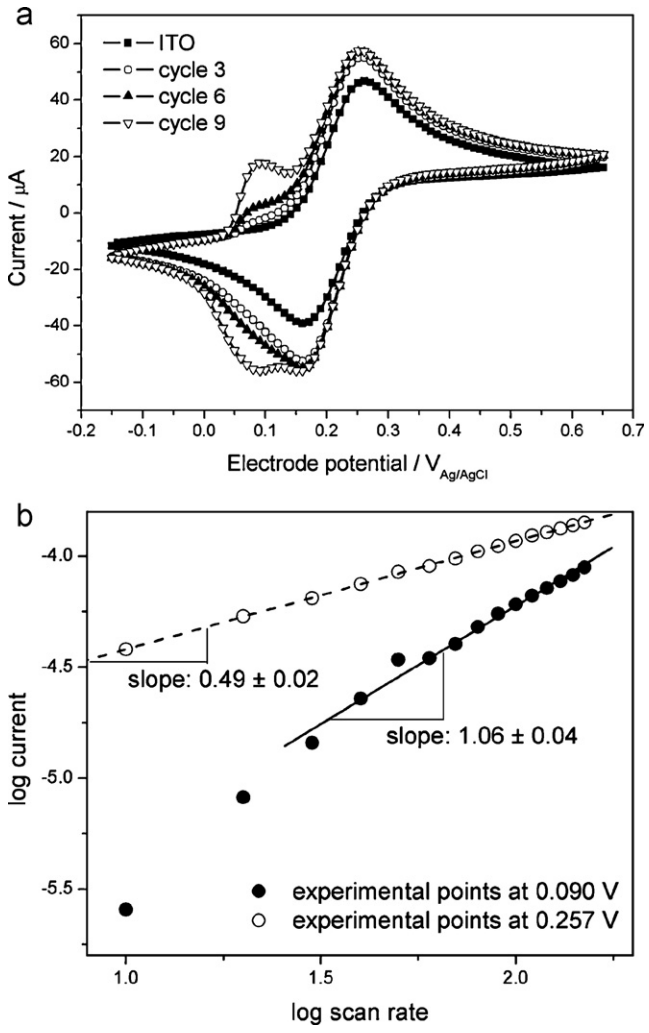

Fig. 9. (a) Cyclic voltammograms of ferrocyanide on a self-assembly depositions of PDADMAC and HPCMs. Electrolyte: 1 M KCl. Scan rate: 50 mV s^{-1}. The alternated adsorption cycles are deposited on ITO glass as a base electrode. (b) Slope of log current versus log scan rate at 0.090 V and 0.257 V corresponding to finite and semi-infinite diffusion, respectively.

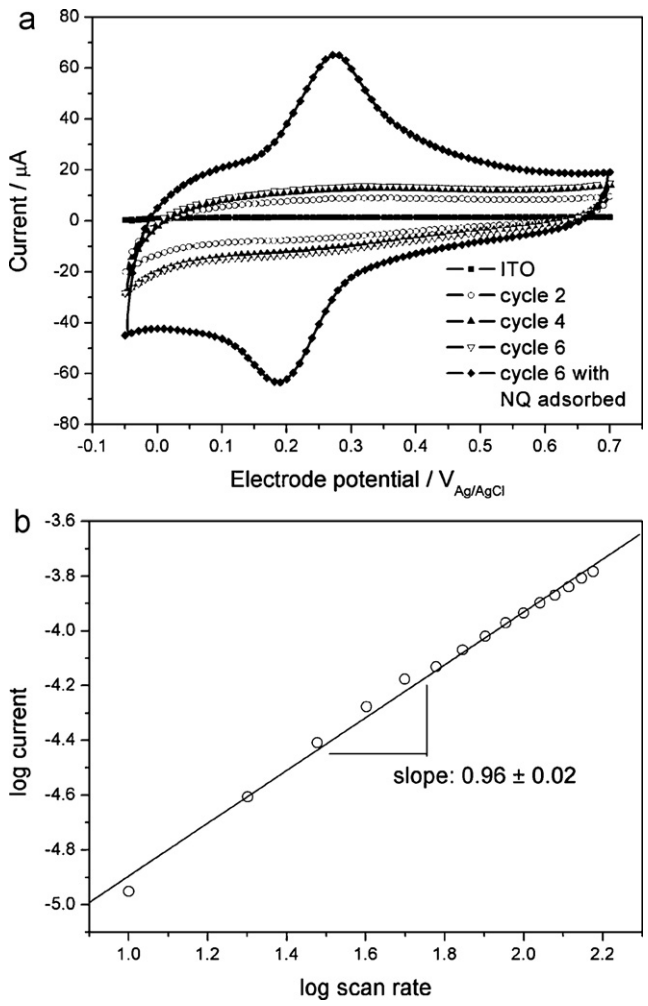

Fig. 10. (a) Cyclic voltammograms of PDADMAC/HPCMs with NQ adsorbed. Electrolyte: 1 M $HClO_4$. Scan rate: 50 mV s^{-1}. The alternated adsorption cycles are deposited on ITO glass as a base electrode. (b) Slope of log current versus log scan rate at 0.278 V corresponding to finite diffusion.

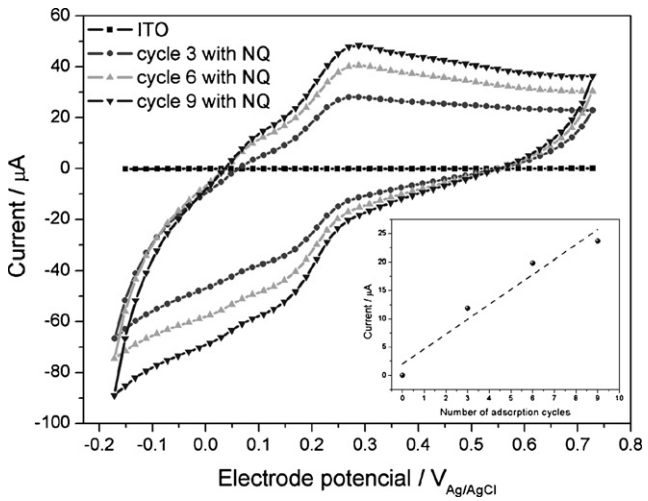

Fig. 11. Cyclic voltammograms of PDADMAC/HPCMs with adsorbed NQ in the third, sixth and ninth adsorption cycles. Electrolyte: 1 M $HClO_4$. Scan rate: 50 mV s^{-1}. The alternated adsorption cycles are deposited on ITO glass as a base electrode. The inset shows the plot of current at 0.280 V versus number of adsorption cycles.

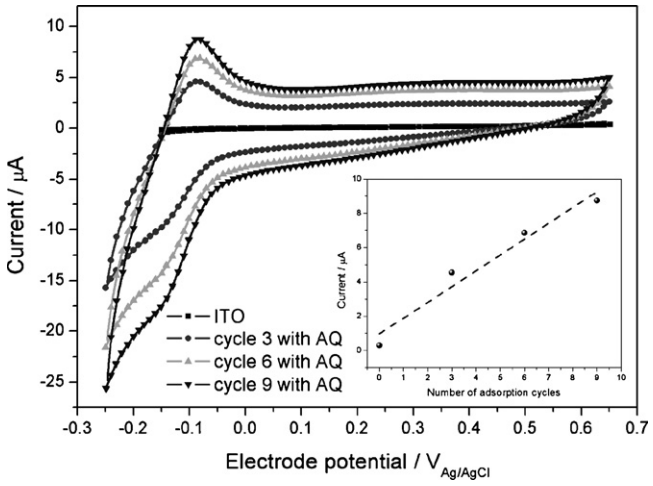

Fig. 12. Cyclic voltammograms of PDADMAC/HPCMs with adsorbed AQ in the third, sixth and ninth adsorption cycles. Electrolyte: 1 M $HClO_4$. Scan rate: 50 mV s^{-1}. The alternated adsorption cycles are deposited on ITO glass as a base electrode. The inset shows the plot of current at −0.082 V versus number of adsorption cycles.

As can be seen in Fig. 12, the current at −0.082 V increases with adsorption cycles process due to the modified electrode shows the redox response of AQ. It also can be seen that the current increases linearly with the number of steps (inset in Fig. 12).

A similar procedure, as described above, was carried out for adsorption of BQ. The electrode was immersed for 30 min in a 10 mM BQ acetonitrile solution after every three adsorption cycles of PDADMAC/HPCMs (Fig. 13).

Fig. 13 shows the increase of current at 0.532 V with number of adsorption cycles. This means that the faradic current corresponding to the redox response of the BQ. Fig. 13 also shows that there is a strong adsorption of BQ and this faradaic current is approximately 40 times higher than faradaic current of adsorbed NQ and AQ shown in Figs. 11 and 12, respectively. Since the BQ molecules are the smallest of three quinones used, a large number of these molecules could be adsorbing on HPCMs, generating a higher current response. Inset in Fig. 13 shows that the current increases linearly with the number of steps.

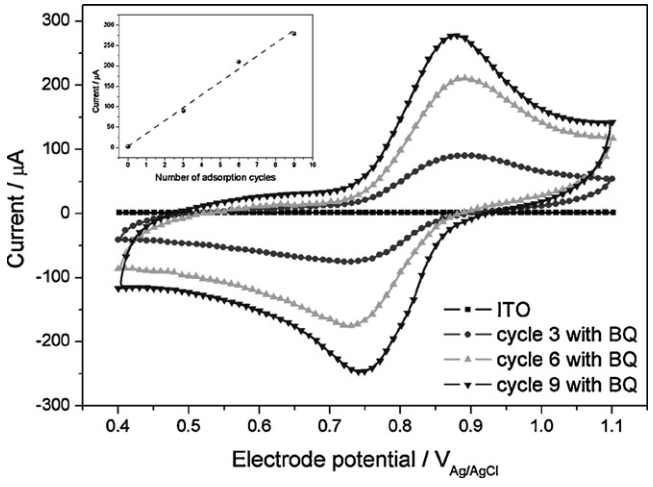

Fig. 13. Cyclic voltammograms of PDADMAC/HPCMs with adsorbed BQ in the third, sixth and ninth adsorption cycles. Electrolyte: 1 M $HClO_4$. Scan rate: 50 mV s^{-1}. The alternated adsorption cycles are deposited on ITO glass as a base electrode. The inset shows the plot of current at 0.532 V versus number of adsorption cycles.

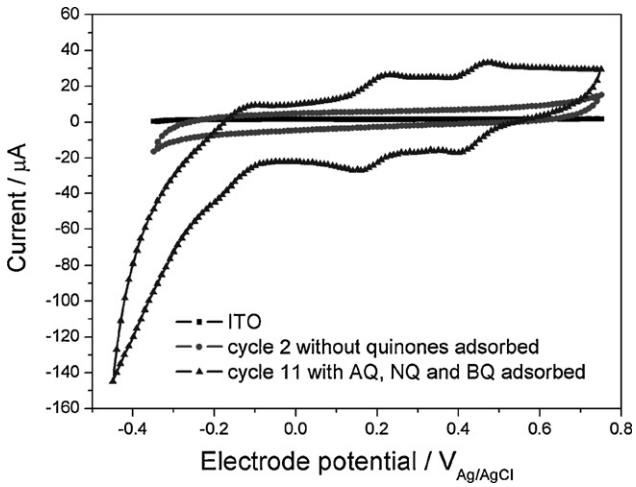

Fig. 14. Cyclic voltammograms of PDADMAC/HPCMs with AQ, NQ and BQ adsorbed in the same electrode. Electrolyte: 1 M $HClO_4$. Scan rate: 50 mV s^{-1}. The alternated adsorption cycles are deposited on ITO glass as a base electrode.

As shown above, it is achievable to built tailored electrodes with pseudocapacitive behavior that working at a specific potential (redox potential of AQ, NQ and BQ).

Finally, we performed an electrode using three different quinones at the same time. After performing the fifth, eighth and eleventh adsorption cycle of PDADMAC/HPCMs, the electrode was immersed for 30 min in 10 mM solutions of AQ, NQ and BQ, respectively. Fig. 14 shows the modified electrode with redox response of all quinones adsorbed.

As shown in Fig. 14, the second adsorption cycle of PDADMAC/HPCMs shows only capacitive current from the increase in the amount of assembled HPCMs, while eleventh adsorption cycle present three different faradaic current, at −0.062 V, 0.271 V and 0.518 V which correspond to the oxidation of AQ, NQ and BQ, respectively. Moreover, the current at 0.518 V decays about 2.6 times respect to the current obtained from Fig. 13, at the same potential. This would indicate that a smaller amount of BQ was adsorbed, possibly because the pores of HPCMs were partially filled with AQ and NQ. However, by ESA process is possible to modify electrodes and significantly increase (more than 4 times) the capacitance. It is noteworthy that the procedure allows to maintain a nearly constant capacitance in the potential range −0.2 to 0.8 V (ΔE = 1 V). Adsorbing a single redox molecule increase the specific charge stored in the electrode but the charge-potential behavior will resemble that of a battery material (e.g. nickel oxide). By adsorbing several redox molecules on different particles of a ESA multilayer it is possible to increase the specific charge with a charge-potential behavior in a capacitive fashion.

4. Conclusions

In summary, the use of CTAB as a pore stabilizer in the reaction media during the sol–gel polycondensation of resorcinol with formaldehyde produces the formation of monolithic porous carbon. Porous carbon microparticles were obtained by milling and sieving monolithic carbon. The pore distribution analysis of nitrogen isotherm data shows that the carbon material presents micro and mesopores, while SEM image of the HPCMs reveals the presence of mesopores and macropores. The BET surface area is 536 m^2 g^{-1}. The specific capacitance and areal capacitance for PCM obtained by EIS measurement reaches values of 194 F g^{-1} and 152 mF cm^{-2}, respectively. However, the cyclic voltammetry experiments at a relatively high scan rate of 100 mV s^{-1}, show that the HPCMs sample present a specific capacitance of 154 F g^{-1} and a high areal

capacitance of ca. 121 mF cm^{-2}, in acid media, making it a useful material in fast supercapacitor applications. Moreover, cyclic voltammograms show that the stepwise electrostatic self-assembly of PDADMAC and carbon microparticles is possible. The amount of carbon material adsorbed could be controlled by controlling the number of adsorption cycles. Normalized surface coverage of HPCMs on ITO electrode correlates well with the measured capacitive current obtained from successive adsorption cycles of PDADMAC and HPCMs.

Oxidation/reduction of a soluble redox probe ($[Fe(CN)_6]^{4-}$) allows detecting the confined diffusion inside the pores and the semi-infinite diffusion on the outer surface of the particles. The high porosity of the HPCMs allow to adsorbs redox molecules (e.g. naphthoquinone) to increase (up to 5 times) the pseudocapacitance of the electrode, to value of ca. 900 F g^{-1}. The value is large compared with those reported in the literature (840 F g^{-1}) [29,30], for more difficult to prepare carbon materials. We have also we demonstrated the potential of ESA process to adsorb three different quinones in a single electrode, increasing more than 4 times the capacitance in a wide range of potential. The pseudocapacitance of the HPCMs layers remains active up to relatively fast scan rates (150 mV s^{-1}). Therefore, this type of modified electrode could be used in supercapacitor devices.

Acknowledgements

This work was funded by FONCYT, CONICET and SECYT-UNRC. J. Balach thanks CONICET for a graduate research fellowship. D. Acevedo and C. Barbero are permanent research fellows of CONICET. Authors would like to thank project partners F. Soldera and F. Mücklich for the help with SEM image.

References

[1] B.E. Conway, Electrochemical Supercapacitors: Scientific Fundamentals and Technological Applications, Kluwer Academic/Plenum Publishers, New York, 1999, pp. 183–220.
[2] F. Beguin, E. Frackowiak, Carbons for Electrochemical Energy Storage and Conversion Systems, CRC Press, Boca Raton, 2009, pp. 426–427.
[3] H. Marsh, F.R. Reinoso, Activated carbon, Elsevier Science, New York, 2005, pp. 38–42.
[4] G. Cao, Nanostructures and Nanomaterials: Synthesis, in: Properties and Applications, Imperial College Press, London, 2004, pp. 247-249.
[5] K.P. Gierszal, T.-W. Kim, R. Ryoo, M. Jaroniec, J. Phys. Chem. B 109 (2005) 23263–23268.
[6] E. Ramasamy, J. Chun, J. Lee, Carbon 48 (2010) 4563–4565.
[7] M.M. Bruno, N.G. Cotella, M.C. Miras, C.A. Barbero, Chem. Commun. (2005) 5896–5898.
[8] R.K. Iler, J. Colloid Interface Sci. 21 (1966) 569–594.
[9] G. Decher, J.-D. Hong, Makromol. Chem. Macromol. Symp. 46 (1991) 321–327.
[10] G. Decher, J.-D. Hong, Ber. Bunsenges. Phys. Chem. 95 (1991) 1430–1434.
[11] H.W. Jomaa, J.B. Schlenoff, Macromolecules 38 (2005) 8473–8480.
[12] E. Blomberg, E. Poptoshev, P.M. Claesson, F. Caruso, Langmuir 20 (2004) 5432–5438.
[13] J.F. Hicks, Y. Seok-Shon, R.W. Murray, Langmuir 18 (2002) 2288–2294.
[14] D.F. Acevedo, J. Balach, C.R. Rivarola, M.C. Miras, C.A. Barbero, Faraday Discuss. 131 (2006) 235–252.
[15] T. Serizawa, H. Takeshita, M. Akashi, Langmuir 14 (1998) 4088–4094.
[16] M.J. Serpe, C.D. Jones, L.A. Lyon, Langmuir 19 (2003) 8759–8764.
[17] M.M. Bruno, N.G. Cotella, M.C. Miras, C.A. Barbero, Colloid Surf. A: Physicochem. Eng. Asp. 362 (2010) 28–32.
[18] S. Brunauer, P.H. Emmett, E. Teller, J. Am. Chem. Soc. 60 (1938) 309–319.
[19] S.J. Gregg, K.S.W. Sing, Adsorption Surface Area and Porosity, 2nd ed., Academic Press, London, 1982.
[20] P.I. Ravikovitch, A.V. Neimark, Colloid Surf. A: Physicochem Eng. Asp. 187–188 (2001) 11–21.
[21] C. Lin, J.A. Ritter, B.N. Popov, J. Electrochem. Soc. 146 (1999) 3639–3643.
[22] D.H. Everett, Pure Appl. Chem. 31 (1972) 577–638.
[23] M. Wiener, G. Reichenauer, T. Scherb, J. Fricke, J. Non-Cryst. Solids 350 (2004) 126–130.
[24] C.R. Hammond, The Elements, CRC Press, Boca Raton, 1994.
[25] J.R. McDonough, J.W. Choi, Y. Yang, F. La Mantia, Y. Zhang, Y. Cui, Appl. Phys. Lett. 95 (2009) 243109.
[26] G.Y. Onoda, E.G. Liniger, Phys. Rev. A 33 (1986) 715–716.
[27] A.J. Bard, L.R. Faulkner, Electrochemical Methods: Fundamentals and Applications, John Wiley and Sons, New York, 1980, pp. 452–558.
[28] A.J. Bard, L.R. Faulkner, Electrochemical Methods: Fundamentals and Applications, John Wiley and Sons, New York, 1980, pp. 228–234.
[29] M. Rose, Y. Korenblit, E. Kockrick, L. Borchardt, M. Oschatz, S. Kaskel, G. Yushin, Small 7 (2011) 1108–1117.
[30] F. Pico, J. Ibañez, M.A. Lillo-Rodenas, A. Linares-Solano, R.M. Rojas, J.M. Amarilla, J.M. Rojo, J. Power Sources 176 (2008) 417–425.